



Tetrahedral framework nucleic acids promote cognitive impairment recovery post traumatic brain injury

Yangyang Wang^{a,1}, Weiqiang Jia^{b,1}, Jianwei Zhu^a, Ruxiang Xu^{a,*}, Yunfeng Lin^{c,*}

^a Department of Neurosurgery, Sichuan Provincial People's Hospital, University of Electronic Science and Technology of China, Chengdu 611731, China

^b Department of Neurosurgery, The First People's Hospital in Shuangliu District/West China Airport Hospital, Sichuan University, Chengdu 610299, China

^c State Key Laboratory of Oral Diseases National Clinical Research Center for Oral Disease, West China Hospital of Stomatology, Sichuan University, Chengdu 610041, China



ARTICLE INFO

Article history:

Received 18 March 2022

Revised 9 August 2022

Accepted 10 August 2022

Available online 14 August 2022

Keywords:

Tetrahedral framework nucleic acids

Traumatic brain injury

Cognitive impairment

Neural stem cell

Neuroinflammation

ABSTRACT

Cognitive impairment often occurs after post traumatic brain injury. In addition, recovery of cognitive impairment is largely dependent on spontaneous repair and the severity of secondary insult. The tetrahedral framework nucleic acid is a novel nanostructure has been shown to have a positive biological effect in promoting regeneration and anti-inflammation. To explore the treatment effect of tetrahedral framework nucleic acids for cognitive impairment recovery post traumatic brain injury, we established a mouse model of traumatic brain injury and verified the efficacy of tetrahedral framework nucleic acids in promoting cognitive impairment recovery post traumatic brain injury. The results show that the tetrahedral framework nucleic acids promoted the recovery of post-traumatic cognitive function by enhancing the proliferation of endogenous neural stem cells. Besides, tetrahedral framework nucleic acids modulated the neuroinflammatory response in the acute phase by inhibiting excessive astrocyte and microglial activation. Taken together, the results of the study indicate tetrahedral framework nucleic acids for treatment of cognitive impairment post traumatic brain injury.

© 2023 Published by Elsevier B.V. on behalf of Chinese Chemical Society and Institute of Materia Medica, Chinese Academy of Medical Sciences.

Traumatic brain injury (TBI) causes large number of deaths and disabilities worldwide every year [1]. According to data from Centers for Disease Control, approximately 2 million TBI patients are recorded every year, and about 50,000 TBI deaths [2]. In addition to death and disability, TBI may also lead to various neurological issues with cognitive impairment as the most common sequelae that can seriously affect the patient's life [3,4]. Cognitive impairment post TBI may last for days to years, and almost all forms of TBI will have a certain degree of spontaneous recovery [5,6]. Therefore, research into new methods to promote cognitive impairment recovery is warranted.

The pathophysiological processes of TBI are very complex and the hippocampal-related physiological circuits, which are involved in cognitive function, are often damaged after TBI [7,8]. Besides the direct hippocampal injury caused by TBI, the inflammatory response following TBI is known to result in secondary insult, which is characterized by astrocytic and microglial activation that, in turn, results in inflammatory cytokine release to creates an inflamma-

tory cascade, resulting in neuronal injury. In the acute phase, microglia and astrocytes undergo a similar morphological alteration, with an initial peak at approximately 3–7 days post TBI [9–12]. Therefore, more effective strategies aimed at inhibiting the over activation of neuroinflammation post TBI are needed.

A neural stem cell (NSC) is a cell that is able to differentiate into multiple central nervous system (CNS) cell types, and which also have long-term capacity for long-term self-renewal [13]. In the adult mammalian brain, there are two main areas that are neurogenic and contain a reservoir of NSCs: the subgranular zone in the hippocampal dentate gyrus and the subventricular zone around the lateral ventricles [13,14]. In recent years, NSC transplantation therapies is increasingly being used to CNS injury and previous studies have shown that NSC transplantation improves cognitive impairment post TBI [15,16]. However, the source of NSCs is an issue worth considering, due to immunosuppression, allergenicity, availability, and possible neoplasia. Indeed, the use of exogenous allogeneic NSCs is greatly limited, hence autologous NSCs have become attractive [17,18]. Endogenous NSCs proliferation is evident after multiple brain injuries including TBI, stroke, and hypoxia; a phenomenon that may be the body's self-healing response to brain injury [17,19–21]. However, the insufficient regeneration capacity of the adult mammalian brain limits the effect of NSC therapy. More-

* Corresponding authors.

E-mail addresses: xuruxiang1123@uestc.edu.cn (R. Xu), yunfenglin@scu.edu.cn

(Y. Lin).

¹ These authors contributed equally to this work.

Table 1
Sequences of ssDNA.

ssDNA	Direction	Base sequence
S1	5'→3'	ATTTATCACCCGCCATAGTACGCTATCACCAGGCAGTTGAGACGAACATTCTAAGTCTGAA
S2	5'→3'	ACATGCGAGGGTCCAATACCGACGATTACAGCTTGCTACACGATTACAGCTTAGGAATGTTCC
S3	5'→3'	ACTACTATGGCGGTGATAAAACGTGTAGCAAGCTGTAATCGACGGGAAGACATGCCCATCC
S4	5'→3'	ACGGTATTGGACCCTCGCATGACTCAACTGCCTGGTGATACGAGGATGGGCATGCTCTTCCCG

over, the local inflammatory niche is not conducive to the proliferation and differentiation of NSCs post injury [22,23]. Therefore, it is necessary to find a new strategy that can not only ameliorate the inflammatory niche but also promote NSC proliferation and differentiation.

With the development of DNA nanotechnology, and based on the principle of base complementary pairing, various spatial DNA nanostructures have been synthesized by using special base sequences. DNA nanotechnology is widely used in disease treatment and diagnosis because of its good biocompatibility and easy editing [24,25]. Tetrahedral framework nucleic acid (tFNA), a new type of DNA nanostructure that has been widely used in biomedicine in recent years due to its simple synthesis and good biological functions [26–28]. The uptake of tFNA by living cells through a caveolin dependent pathway is more efficient than that of single strand nucleic acids, making it a good drug vector to increase efficacy of drugs [25,29]. Besides the potential to be a drug vector, tFNA exhibits possible stem cell proliferation and anti-inflammation capabilities [26,30–32]. Taken together, the current studies suggest that tFNA may be a potential drug for cognitive impairment post TBI. In order to understand the protective and restorative effect of tFNA on cognitive impairment after brain injury and its potential mechanism, a mouse experiment was conducted to test our hypothesis.

We used the methods reported in previous studies to synthesize tFNAs [30,31]. In brief, we mixed the four single strands DNA (ssDNA) with the Tris-MgCl₂ buffer, and the concentration of ssDNA was 1 μmol/L, then the mixtures were put into the PCR instrument to react at 95 °C for 10 min and cool to 4 °C for 20 min. The base sequences of the four ssDNAs (S1, S2, S3, and S4) are shown in Table 1.

To verify the successful synthesis of nano materials. Capillary gel electrophoresis and polyacrylamide gel electrophoresis (PAGE) was used to measure molecular weight of different components, and indirectly reflect the successful synthesis of tFNAs. The sizes, zeta potential, and morphological characteristics of the tFNAs were also detected by dynamic light scattering (DLS) and transmission electron microscopy (TEM).

We collected NSCs from E15.5 embryos as previous described and cultured NSCs in Dulbecco's Modified Eagle Medium/Neuralbasal mixed medium added with 2% B27 supplement, basic fibroblast growth factor (20 ng/mL), and epidermal growth factor (20 ng/mL). After 5 days of culture, NSC spheres were collected by centrifugation [33,34]. The cells were subcultured twice a week, and the second to fourth generations of cells were collected for experiments.

To confirm that tFNA could be uptake by NSCs. The neurospheres of NSCs were dissociated to a single-cell suspension and re-plated onto 24-well dishes pretreat with laminin. After 24 h incubation, the NSCs adhered to dishes, then Cy5-tFNAs with a concentration of 100 μmol/L were added to NSCs medium for 6 h. after that, the residual Cy5-tFNAs were washed 3 times with PBS to remove as much as possible, paraformaldehyde fixation for 30 min at 4 °C, and incubated with Nestin antibody, a specific antibody against neural stem cells overnight at 4 °C, the next day, the samples were incubated with diluted fluorescent secondary antibodies at room temperature for 1 h, and nucleus were dyed with 4',6-diamidino-2-phenylindole (DAPI) for 10 min. Finally, samples fluo-

rescence images were acquired by a laser scanning confocal microscope.

The CCK-8 assay was used to evaluate the efficacy of tFNA on NSCs cells proliferation. Cells were cultured in 96-well plates (5×10^4) with NSC culture medium. Afterward, 62.6, 125, 250, and 350 nmol/L tFNA were mixed to the medium for 24 and 48 h. After washing with PBS for 3 times, the CCK8 was mixed with the NSCs, and then detected at 450 nm by microplate reader.

For animal experiment, mice were purchased from Chengdu Dossy Experimental Animals of China. The pregnant female ICR mice were used for collection of fetal NSCs on E15, and nude mice were used for small animal *in vivo* imaging, while 28–32 g 8-week male ICR mice were used for TBI model. All mice were maintained in a 12:12 h day-night pattern and easy to get food and water. All animal experiments were conducted according to the guidelines of the Animal Ethics Committee of State Key Laboratory of Oral Diseases National Clinical Research Center for Oral Disease, West China Hospital of Stomatology, Sichuan University, Chengdu.

And a distribution experiment of tFNA *in vivo* was conducted as previous described, hairless 8 weeks old male mice (nude mice, BALB/c) were injected with 100 μL Cy5-tFNA (1 μmol/L) by caudal vein to evaluate tFNA distribution of tFNA *in vivo*. Then a whole-body fluorescence system was used for collecting *in vivo* distribution images of Cy5-tFNA at 10, 20, 30, 40, 50 and 60 min after injection [35]. And to determine that tFNA could cross the blood-brain barrier, ICR mice were injected with Cy5-tFNA for 2–3 h, then anesthetized with chloral hydrate and sacrificed the mice. Subsequently a series of 14 μm thick frozen sections were then cut and respectively incubated phalloidin for 30 min and stained nuclei with DAPI for 10 min. And tissue fluorescence images were acquired by laser scanning confocal microscope.

In order to explore the efficacy of tFNA in TBI animals, a standard animal model of TBI was established as previous described [36]. Briefly, mice were randomly divided into three groups (Control, TBI + saline, and TBI + tFNA). And we anesthetized mice with chloral hydrate, then fixed mice to a stereotactic apparatus and the scalp was cut along the midline, followed by a 5 mm × 5 mm craniectomy opened between bregma and lambda, 1 mm outside of the midline. Then a stainless-steel tip of 3 mm size was used to hit the cerebral cortex to produce TBI with a constant speed of 4.4 m/s. After injury, the scalp was sutured using a fine surgical suture, and the mice were subsequently placed in a 37 °C incubator for recovery. And the mice in the control group only underwent craniotomy, but there was no impact injury to the brain tissue. To explore the proliferation of NSCs *in vivo*, BrdU all mice were injected 50 mg/kg BrdU by intraperitoneal injection each day post TBI for 15 days after surgery [37]. Besides, mice in the TBI + saline group were injected with 100 μL saline by caudal vein while mice in the TBI + tFNA group were treated with 100 μL tFNA (1 μmol/L).

To detect pathological changes in the brain. Frozen sections of brain tissue were obtained after sacrificed mice. Subsequently a series of 14 μm thick frozen sections were cut. And frozen sections were permeabilized with 0.1% Triton X-100 (v/v) for 30 min and blocked in 10% FBS and for 1 h, then frozen sections were incubated with diluted primary antibody (Sox2, Brdu, DCX, GFAP, Iba1 primary antibody) overnight at 4 °C, the next day, fluorescent secondary antibody is used to color the primary antibody at room

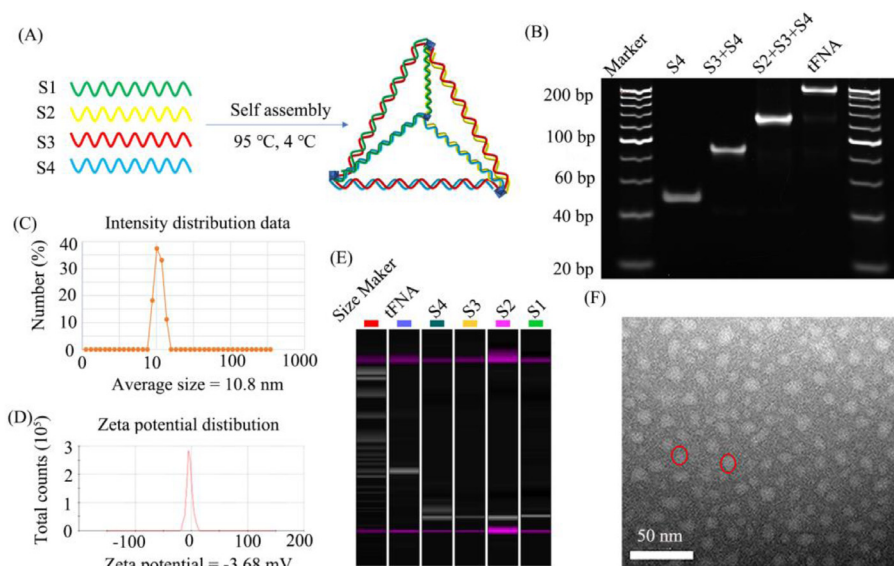


Fig. 1. Successful synthesis of tFNAs. (A) Schematic diagram of tFNA fabrication. (B) PAGE assay of tFNA. (C) Hydrodynamic size of tFNA detected by DLS. (D) Zeta potential of tFNA. (E) Successful synthesis of tFNA was confirmed by capillary gel electrophoresis (CGE). (F) TEM image of tFNAs.

temperature for 1 h, and nucleus was dyed with DAPI for 10 min. After each step, all residual reagents were rinsed by PBS for 3–5 times. Finally, tissue immunofluorescence results were acquired by a laser scanning confocal microscope.

To evaluate the apoptosis of cells *in vivo*, TUNEL (TdT-mediated dUTP nick-end labeling) apoptosis assay kit was used to detect the cell apoptosis of tissue frozen section according to the instruction. The nuclei were counterstained with DAPI. And fluorescent staining image of TUNEL staining were viewed with fluorescence microscopy. TUNEL-positive cells were counted for testing cell apoptosis.

The expression of protein was detected by western blot. Tissue or cells was lysed on ice to obtain total protein and the bicinchoninic acid method was used for protein concentration quantification. SDS-PAGE electrophoresis was used to separate proteins with different molecular weights, then protein was transferred onto nitrocellulose membranes, and blocked by 5% bovine serum albumin for 1 h. Afterwards, nitrocellulose membranes was incubated with the diluted primary antibody (GAPDH, Wnt2, GSK3, β -catenin, TNF α , IL1 β , IL6, caspase3, cleaved caspase3) at a 4 °C refrigerator overnight, the next day, the HRP conjugated secondary antibodies were used to mark the primary antibody. Subsequently the development of immunoactive bands was completed by bio rad detection system. At last, the images were processed by ImageJ software.

Finally, the Morris Water Maze (MWM) was used to verify whether tFNA can improve the cognitive impairment of experimental animals, MWM was carried out as previous described [38]. Briefly, we divided a pool with a diameter of one meter into four quadrants, and pasted different labels on the wall of each quadrant as a sign for mice to identify the direction. The temperature of the pool was maintained at about 20 °C, and lithium dioxide was added to the water for animal tracking. We carried out the test at the same time every afternoon and ensured that the test was carried out in a quiet and no strong light test environment. For Hidden Platform Test, each mouse was put into the pool at different quadrants, and its trace and time for finding the hidden platform under the water were recorded. If the mice still did not find the hidden platform for more than 60 s, the experiment is terminated, and the mice will be actively put on the hidden platform under the pool for 10 s, the time for these mice to find the plat-

form was uniformly recorded as 60 s. On the 6th day, the probe trial was conducted after finishing the Hidden Platform Test. The hidden platform under the water was moved away, then we put the mice into the water from the opposite quadrant where the platform was located, and observed and recorded their movement trajectory in the pool for 60 s. The time of mice in the target quadrant and the number of times they cross the location of platform were used as indicators to evaluate their spatial memory.

GraphPad Prism software 8 was used for statistical tests. Statistical significance between the two groups were calculated by Student's *t*-test. Values of $P < 0.05$ represented statistically significance. Data were expressed as mean \pm standard deviation (SD).

Synthesis of tFNA by four ssDNA was shown in Fig. 1A. PAGE results showed that there was nucleic acid on the 200 bp band, which was just equal to the sum of the molecular weights of the four ssDNA, indirectly indicating that four ssDNA were successfully combined that we successfully synthesized the tFNA, and the results also indicated that the molecular weights of tFNA was approximately 200 bp (Fig. 1B). DLS was utilized to detect the size of tFNA, with results demonstrating that the hydrodynamic diameter of tFNA was approximately 10.8 nm and the zeta potential was approximately -3.68 mV (Figs. 1C and D). After, we further used capillary gel electrophoresis to verify that tFNAs were successfully synthesized. The results verified by capillary gel electrophoresis were in accord with the PAGE results (Fig. 1E). Transmission electron microscope (TEM) was used to confirm the nanostructure, and a tetrahedron nanostructure with a diameter of about 10 nm was observed (Fig. 1F). These results show that the tetrahedron nanostructure met our expected design and was consistent with our previous results [35,39].

After treating with tFNA-Cy5 for 6 h, and a colocalized fluorescence signal for NSCs and tFNA was found (Fig. 2A), this result demonstrated that tFNA was taken up by NSCs. After treating with tFNA for 24 or 48 h, CCK-8 assays showed that tFNA enhanced NSC proliferation and that the optimal concentration of tFNA was 250 nmol/L (Fig. 2B), which was similar to previous results [30]. In addition, more NSC spheres were observed in tFNA group compared with PSB group under the microscope (Fig. 2C). To elucidate the mechanism through which tFNA promotes NSC proliferation, we used western blot to determine the expression of proteins related to the Wnt/ β -catenin/GSK3 pathway, a path-

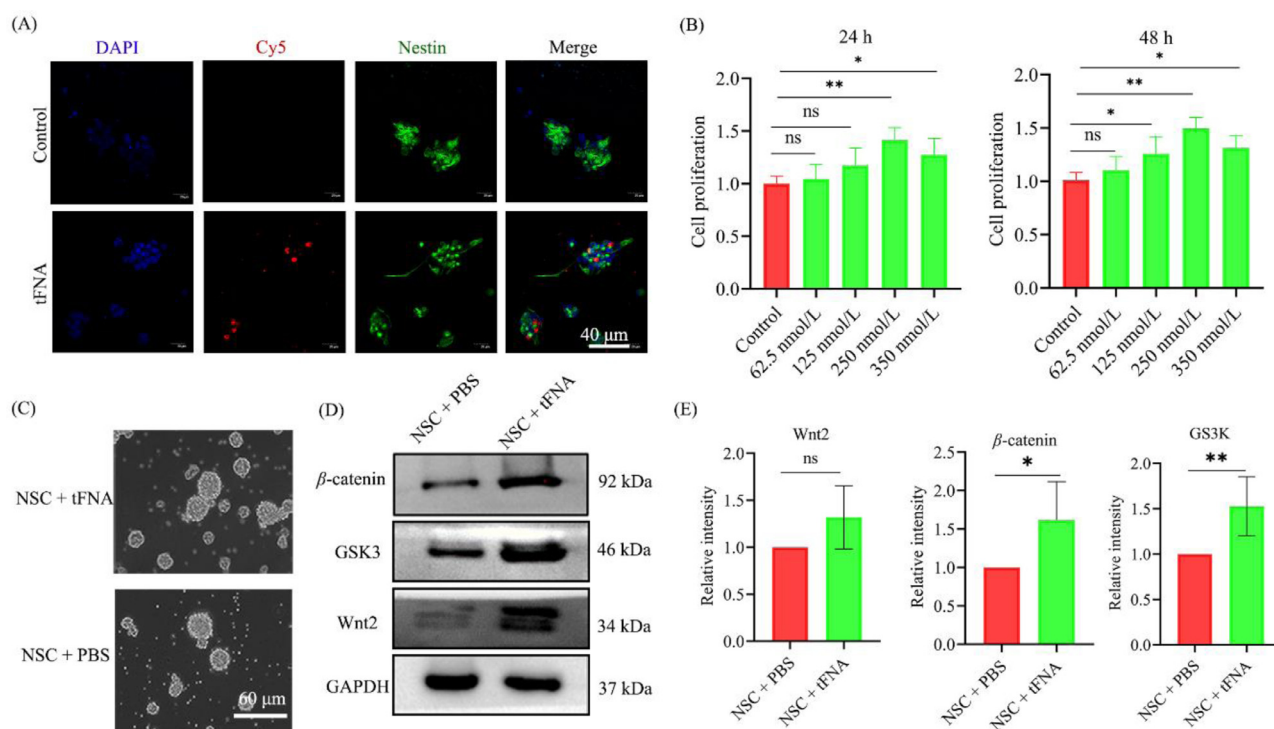


Fig. 2. tFNA could promote neural stem cell proliferation *in vitro*. (A) Uptake of Cy5-tFNA by NSCs. (B) CCK8 assay to evaluate the effect of tFNA on NSCs proliferation at 24 h and 48 h. (C) Representative microscopic growth of NSCs spheres. (D, E) Expression level of Wnt/ β -catenin/GSK3 protein by Western blot. Data are presented as mean \pm SD ($n=5$); * $P < 0.05$, ** $P < 0.01$, ns = no significance.

way related to the cell cycle, with results indicating that enhanced Wnt/ β -catenin/GSK3 expression was evident in the tFNA group compared with PBS group (Figs. 2D and E). Previous results showed that tFNA enhanced stem cell proliferation by Wnt/ β -catenin pathway [35,40]. To sum up, our results demonstrated that tFNA was a good biological nanostructure that can promote the proliferation of NSCs *in vitro*.

After treating with tFNA for 15 days, the MWM test was performed and the swimming track was recorded. The results of hidden platform test showed that the escape latency of mice in the TBI+tFNA group was obviously reduced compared with TBI+saline group (Figs. 3A and B). And no significant difference of the mice swimming velocity was observed in different groups (Fig. 3C). This suggests that treating with tFNA could ameliorate the memory ability of mice post TBI. The probe trial was conducted on the 6th day, the platform was removed, and the swimming track of mice in the pool were recorded for 60 s (Figs. 3D–F). The swimming track of mice in the TBI+ tFNA group indicated that the mice stayed longer in the target quadrant than did mice in the TBI+saline group (Figs. 3D and E). Moreover, the numbers of crossing the platform location increased significantly (Fig. 3F). These data confirm that tFNA treatment significantly improved cognitive performance in ICR mice post TBI.

Next, we verified that tFNA successfully penetrated the blood-brain barrier. *In vivo* imaging system showed that tFNA accumulated in the brain and last for more than 1 h (Fig. 4A). Moreover, fluorescence staining results of brain tissue frozen sections clearly confirmed that tFNA entered the brain and was taken up by cells. Specifically, the Cy5-tFNA fluorescence signal was detected in hippocampal and cortical cells (Fig. 4B). Due to the existence of blood-brain barrier, various drugs are not able to enter the brain, which reduces the potential therapeutic effects. Drugs with molecular weights greater than 400 Da are usually too large to penetrate the blood-brain barrier [41]. However, results from our study demonstrated that tFNA was able to penetrate the blood-brain barrier.

After treatment with tFNA for 15 days post TBI, Sox2 and BrdU staining which were indicators of cell proliferation were used to assess NSC proliferation, after treating with tFNA, more Sox2 positive cells were observed in the dentate gyrus (DG) of mice, while less Sox2 positive cells observed after treating with saline (Figs. 4C and D). Furthermore, more Sox2 and BrdU double positive cells were observed in TBI+tFNA group than in the TBI+saline group (Figs. 4C and E). In addition, immunofluorescence staining of doublecortin (DCX), a marker of newborn neurons, the numbers of DCX positive cells were increased in the DG of mice in the TBI+tFNA group compared with that of mice in the TBI+saline group; what's more, the neurite branches of newborn neurons were similar with those of the control group (Figs. 4F–H). Our previous studies have demonstrated that tFNA enhanced NSC proliferation *in vitro* [30,35,42]. Here, we showed that tFNA could be a good potential nanomaterial by enhance endogenous NSC proliferation, and this can well avoid the problems of immunogenicity and tumorigenicity in the treatment of exogenous cells to some extent.

As neuroinflammatory response cells, astrocytes and microglia are involved in the neuroinflammatory response of the CNS. To explore the anti-inflammatory effects of tFNA, some indicators related to neuroinflammation were detected. First, we determined the expression levels of the astrocyte marker GFAP and microglial marker Iba1. Compared with the saline treatment group, immunofluorescence staining results showed that tFNA reduced the expression of GFAP in the hippocampi of mice (Figs. 5A and C). Similarly, the expression of Iba1 post TBI was also reduced after treating with tFNA compared with the saline treatment group (Figs. 5B and D). The levels of proinflammatory cytokines indicate, to some extent, the degree of inflammation. To verify our assumption, TNF α , IL1 β and IL6 expression levels were determined by western blot. Results indicated that fewer proinflammatory cytokines were detected after treating with tFNA post TBI compared with the saline treatment group (Figs. 5G and I). In addition, treating with tFNA reduced the number of TUNEL-positive hippocam-

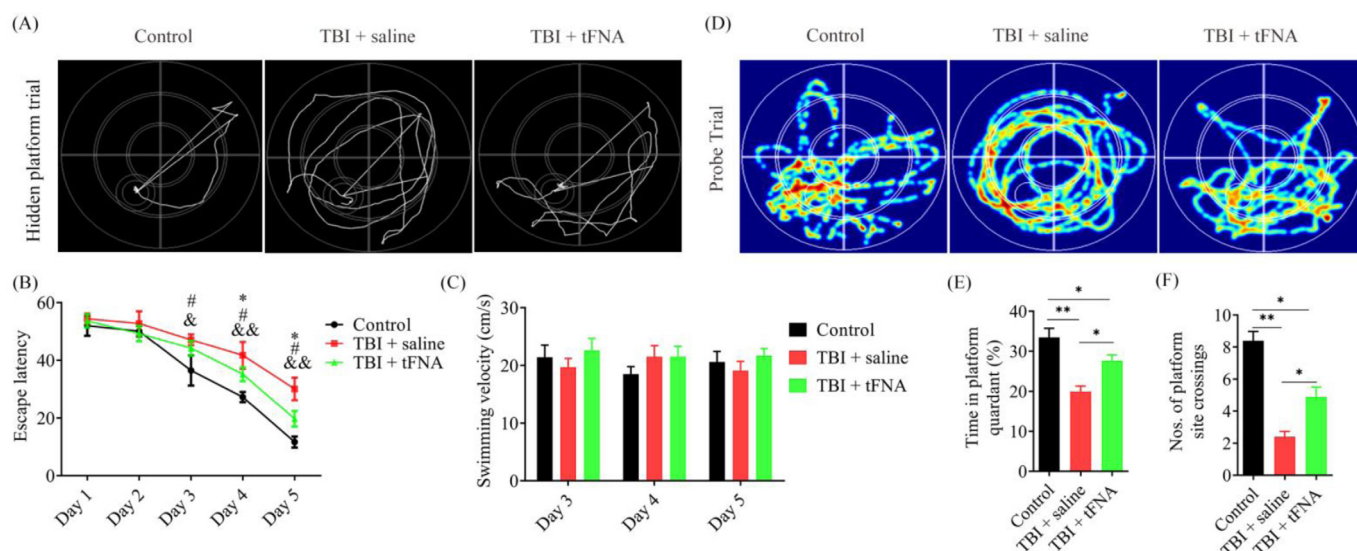


Fig. 3. Behavioral evaluation of tFNA nanostructure therapy in ICR mice by MWM. (A) Representative swimming track of hidden platform test. (B) Statistical analysis of the escape latency. * $P < 0.05$ (TBI + saline vs. TBI + tFNA), # $P < 0.05$ (Control vs. TBI + tFNA), & $P < 0.05$ (Control vs. TBI + saline), && $P < 0.01$ (Control vs. TBI + saline). (C) Swimming velocity. (D) Representative swimming track of spatial probe trial. (E) Residence time of mice in target quadrant. (F) Number of crossing the platform location of each group on the probe trial day. Data are presented as mean \pm SD ($n = 5$); * $P < 0.05$, ** $P < 0.01$, *** $P < 0.001$.

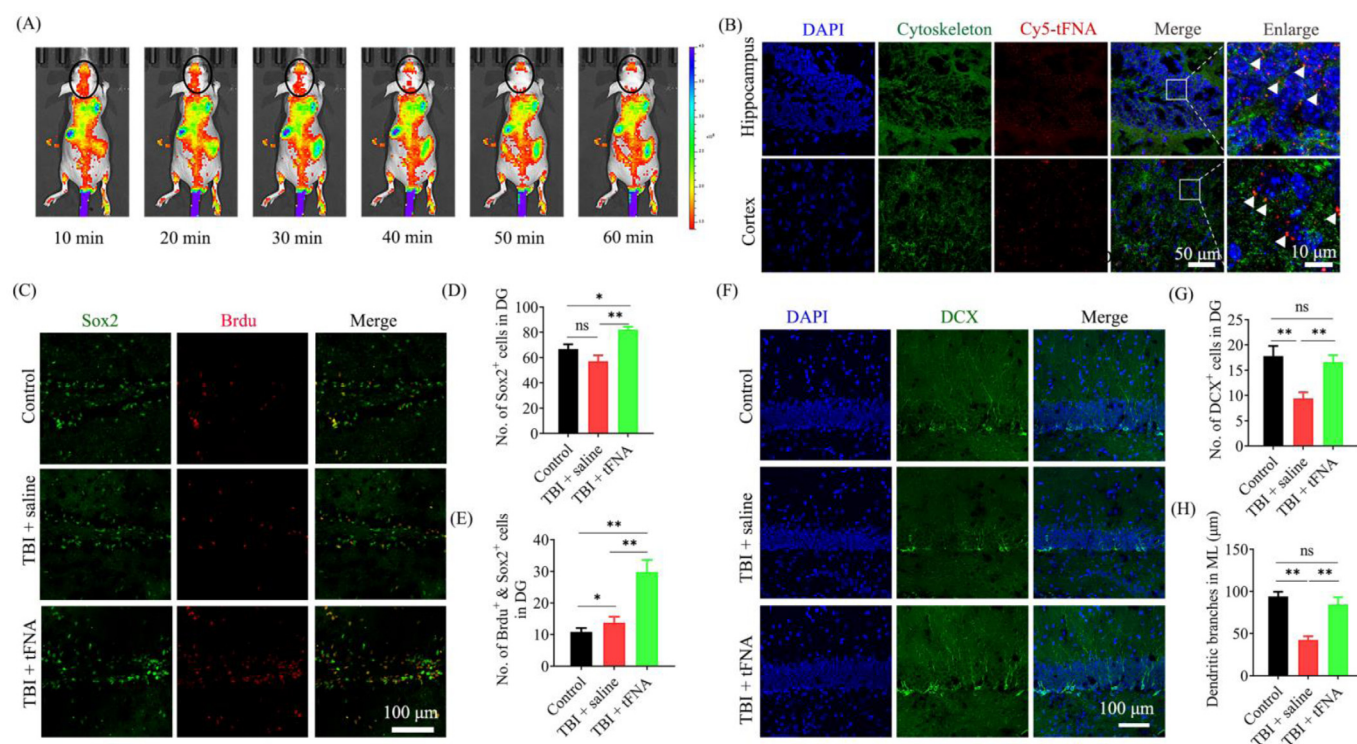


Fig. 4. tFNA distribution *in vivo* and tFNA promote neuro regeneration *in vivo*. (A) *In vivo* fluorescent signal images at different time point after Cy5-tFNA was injected into BALB/c nude mice. (B) Representative fluorescence images of Cy5-tFNA (red) brain sections in hippocampus and cerebral cortex. (C, D, E) Representative immunofluorescence images of Sox2 (green) and Brdu (red) staining in dentate gyrus of hippocampus. (F, G, H) Representative immunofluorescence images of DCX staining in dentate gyrus of hippocampus. Data are presented as mean \pm SD ($n = 5$); * $P < 0.05$, ** $P < 0.01$, ns = no significance.

pal cells compared with the mice treating with saline (Figs. 5E and F). Furthermore, apoptosis related proteins activated caspase3 expression were determined by western blot, and lower level of the apoptotic protein was observed after treating with tFNA compared with saline treatment (Figs. 5H and J). Previous studies have shown that overactivated astrocytes mediate the neuroinflammatory response by multiple mechanisms [43,44]. Similarly, microglia are known to be inherent immune effector cells that mediate the neu-

roinflammatory response in the CNS [9]. Our results demonstrated that tFNA modulated the neuroinflammatory response by inhibiting activation of both astrocytes and microglia. And inhibiting neuroinflammation overactivation was closely related with apoptosis [9,45,46]. In all, our results show that the tFNA can display a good anti-inflammatory and anti-apoptotic effect post TBI.

Cognitive impairment is a common neurological sequela post TBI, and the recovery of cognitive impairment depends on the neu-

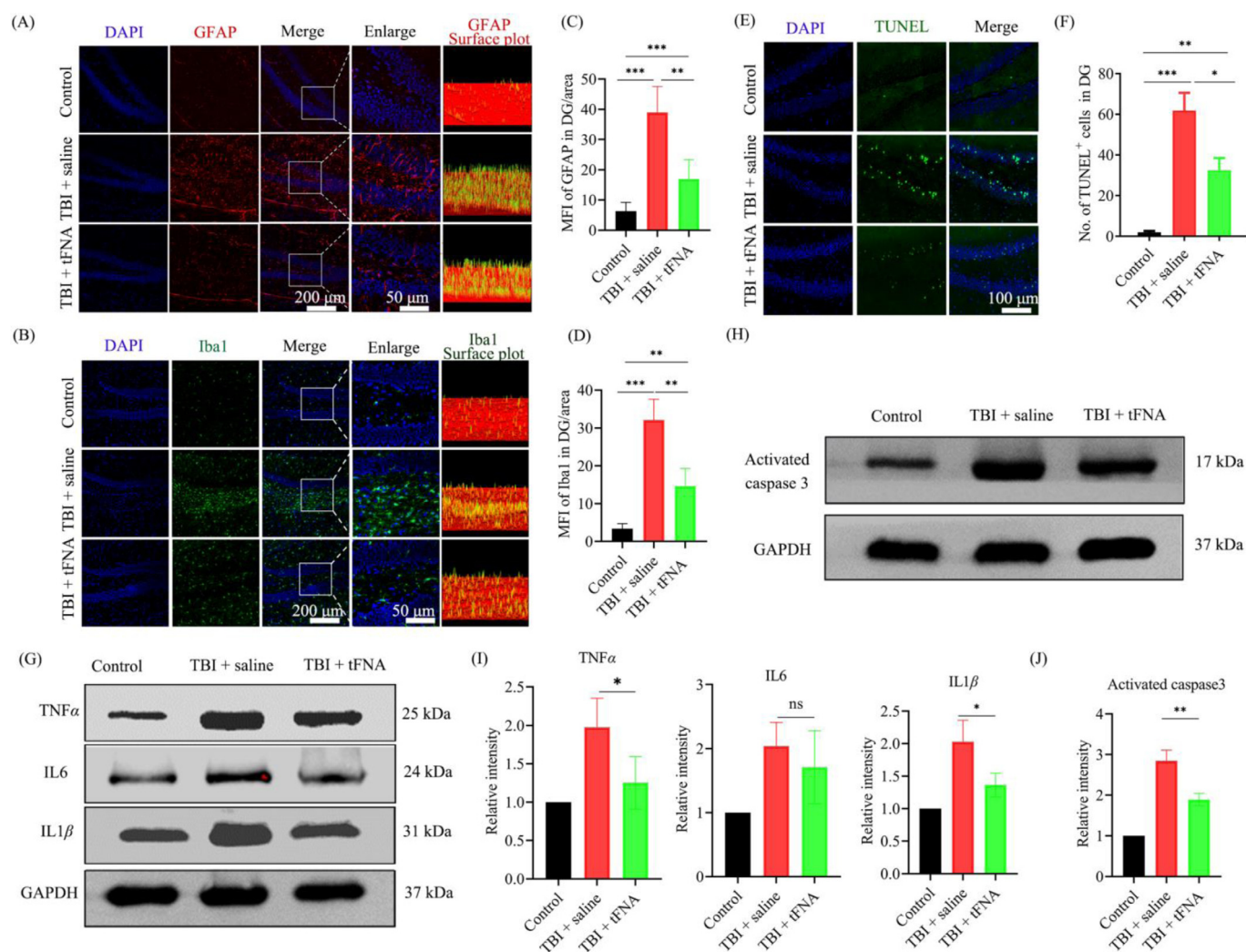


Fig. 5. The anti-inflammatory and anti-apoptotic effects of tFNAs. (A) Immunofluorescence images of GFAP (red) protein in hippocampus dentate gyrus (DG) of traumatic brain injury after 3 days treatment. (B) Immunofluorescence images of Iba1 (green) protein in hippocampus dentate gyrus (DG) of traumatic brain injury after 3 days treatment. (C) Mean fluorescence intensity (MFI) of GFAP in DG. (D) Mean fluorescence intensity (MFI) of Iba1 in DG. (E) TUNEL (green) staining in hippocampus dentate gyrus (DG). (F) Statistical analysis of cells apoptosis by TUNEL staining in DG of TBI mice after 3 days treatment. (G) Expression level of TNF α , IL6 and IL1 β as analyzed using Western blot. (H) Expression level of caspase3 and active caspase3 by Western blot. (I) Statistical analysis of expression level of TNF α , IL6 and IL1 β . (J) Statistical analysis of expression level of active caspase3. Data are presented as mean \pm SD ($n=5$); * $P < 0.05$, ** $P < 0.01$, *** $P < 0.001$, ns = no significance.

regeneration ability of the organism and secondary insult caused by neuroinflammatory response. Our study initially demonstrated that tFNA promoted cognitive impairment recovery by enhancing endogenous NSC proliferation. In addition, tFNA ameliorated the neuroinflammatory response by inhibiting excess activation of both astrocytes and microglia. Therefore, tFNA could be a potential drug for promoting cognitive impairment recovery post TBI.

Declaration of competing interest

The authors declare that they have no known competing financial interests or personal relationships that could have appeared to influence the work reported in this paper.

Acknowledgments

This work was supported by the National Key R&D Program of China (No. 2019YFA0110600), the National Natural Science Foundation of China (Nos. 81970916, 81971295, 92001216, 82171355), the China Postdoctoral Science Foundation (No. 2021M700699), Sichuan Province Youth Science and Technology Innovation

Team (No. 2022JDTD0021) and Research Funding from West China School/Hospital of Stomatology Sichuan University (No. RCDWJS2021-20).

References

- [1] A.I. Maas, N. Stocchetti, R. Bullock, *Lancet Neurol.* 7 (2008) 728–741.
- [2] A. Capizzi, J. Woo, M. Verduzco-Gutierrez, *Med. Clin. North. Am.* 104 (2020) 213–238.
- [3] J. Nicholl, W.C. LaFrance, *Semin. Neurol.* 29 (2009) 247–255.
- [4] J.E. Pierce, D.H. Smith, J.Q. Trojanowski, T.K. McIntosh, *Neuroscience* 87 (1998) 359–369.
- [5] C.B. Peltz, K. Kenney, J. Gill, et al., *Neurology* 95 (2020) e1126–e1133.
- [6] C.A. Blaiss, T.S. Yu, G. Zhang, et al., *J. Neurosci.* 31 (2011) 4906–4916.
- [7] D.I. Graham, J.H. Adams, J.A. Nicoll, W.L. Maxwell, T.A. Gennarelli, *Brain Pathol.* 5 (1995) 397–406.
- [8] J.H. Adams, D. Doyle, I. Ford, et al., *Histopathology* 15 (1989) 49–59.
- [9] D.W. Simon, M.J. McGeachy, H. Bayir, et al., *Nat. Rev. Neurol.* 9 (2017) 171–191.
- [10] J.E. Burda, A.M. Bernstein, M.V. Sofroniew, *Exp. Neurol.* 13 (2016) 305–315.
- [11] Z. Zhang, J.S. Zoltewicz, S. Mondello, et al., *PLoS One* 3 (2014) e92698.
- [12] T. Frugier, M.C. Morganti-Kossmann, D. O'Reilly, C.A. McLean, *J. Neurotrauma* 9 (2010) 497–507.
- [13] B.A. Reynolds, S. Weiss, *Science* 255 (1992) 1707–1710.
- [14] J.P. Andreotti, W.N. Silva, A.C. Costa, et al., *Semin. Cell Dev. Biol.* 95 (2019) 42–53.
- [15] D.L. Haus, L. Lopez-Velazquez, E.M. Gold, et al., *Exp. Neurol.* 281 (2016) 1–16.

- [16] G.R. Bjorklund, T.R. Anderson, S.E. Stabenfeldt, *Int. J. Mol. Sci.* 4 (2021) 1978.
- [17] R.M. Richardson, A. Singh, D. Sun, et al., *J. Neurosurg.* 112 (2010) 1125–1138.
- [18] I. Kulbatski, A.J. Mothe, H. Nomura, C.H. Tator, *Curr. Drug Targets* 6 (2005) 111–126.
- [19] S. Chirumamilla, D. Sun, M.R. Bullock, R.J. Colello, *J. Neurotrauma* 19 (2002) 693–703.
- [20] P.K. Dash, S.A. Mach, A.N. Moore, *J. Neurosci. Res.* 63 (2001) 313–319.
- [21] D. Sun, *Exp. Neurol.* 3 (2016) 405–410.
- [22] M.L. Monje, H. Toda, T.D. Palmer, *Science* 302 (2003) 1760–1765.
- [23] R.E. Iosif, C.T. Ekdahl, H. Ahlenius, et al., *J. Neurosci.* 26 (2006) 9703–9712.
- [24] S. Ranallo, A. Porchetta, F. Ricci, *Anal. Chem.* 91 (2019) 44–59.
- [25] T. Zhang, T. Tian, R. Zhou, S. Li, *Nat. Protoc.* 8 (2020) 2728–2757.
- [26] X. Yang, F. Zhang, Y. Du, et al., *Chin. Chem. Lett.* 33 (2022) 1901–1906.
- [27] Mi Zhou, T. Zhang, B. Zhang, et al., *ACS Nano* 16 (2022) 1456–1470.
- [28] W. Ma, Y. Zhan, Y. Zhang, et al., *Signal Transduct. Target Ther.* 6 (2021) 351.
- [29] J.Li L.Liang, Q. Li, et al., *Angew. Chem. Int. Ed.* 53 (2014) 7745–7750.
- [30] T. Chen, D. Xiao, Y. Li, et al., *Chin. Chem. Lett.* 33 (2022) 2517–2521.
- [31] M. Zhou, N.X. Liu, S.R. Shi, et al., *Nanomedicine* 14 (2018) 1227–1236.
- [32] T. Zhang, T. Tian, Y. Lin, *Adv. Mater.* 34 (2022) 2107820.
- [33] T. Suehara, J. Morishita, M. Ueki, et al., *Paediatr. Anaesth.* 26 (2016) 52–59.
- [34] C. Liang, F. Du, J. Wang, J. Cang, Z. Xue, *Anesth. Analg.* 129 (2019) 608–617.
- [35] W. Ma, Y. Zhan, Y. Zhang, et al., *ACS Appl. Mater. Interfaces* 12 (2020) 2095–2106.
- [36] S.G. Kernie, T.M. Erwin, L.F. Parada, *J. Neurosci. Res.* 66 (2001) 317–326.
- [37] S.R. Ferron, C. Andreu-Agullo, H. Mira, et al., *Nat. Protoc.* 2 (2007) 849–859.
- [38] Y. Zhou, F. Zhu, Y. Liu, et al., *Sci. Adv.* 6 (2020) eabc7031.
- [39] W. Cui, Y. Zhan, X. Shao, et al., *ACS Appl. Mater. Interfaces* 11 (2019) 32787–32797.
- [40] Q. Peng, X.R. Shao, J. Xie, et al., *ACS Appl. Mater. Interfaces* 8 (2016) 12733–12739.
- [41] T.D. Azad, J. Pan, I.D. Connolly, A. Remington, C.M. Wilson, G.A. Grant, *Neurosurg. Focus* 38 (2015) E9.
- [42] Y. Gao, T.X. Zhang, J.Y. Zhu, et al., *Mater. Chem. Front.* 4 (2020) 2731–2743.
- [43] A. Litvinchuk, Y.W. Wan, D.B. Swartzlander, et al., *Neuron* 100 (2018) 1337–1353.
- [44] M. Linnerbauer, M.A. Wheeler, F.J. Quintana, *Neuron* 108 (2020) 608–622.
- [45] R.G. Mira, M. Lira, W. Cerpa, *Front. Physiol.* 12 (2021) 740939.
- [46] J. Zhu, Y. Yang, W. Ma, Y. Wang, et al., *Nano Lett.* 22 (2022) 2381–2390.